ARTICLES
https://doi.org/10.1038/s41559-018-0768-z
nature ecology & evolution

Fibroblasts and alectinib switch the evolutionary games played by non-small cell lung cancer

Artem Kaznatcheev[1,2*], Jeffrey Peacock[3], David Basanta[4], Andriy Marusyk[5*] and Jacob G. Scott[2,6*]

Heterogeneity in strategies for survival and proliferation among the cells that constitute a tumour is a driving force behind the evolution of resistance to cancer therapy. The rules mapping the tumour's strategy distribution to the fitness of individual strategies can be represented as an evolutionary game. We develop a game assay to measure effective evolutionary games in co-cultures of non-small cell lung cancer cells that are sensitive and resistant to the anaplastic lymphoma kinase inhibitor alectinib. The games are not only quantitatively different between different environments, but targeted therapy and cancer-associated fibroblasts qualitatively switch the type of game being played by the in vitro population from Leader to Deadlock. This observation provides empirical confirmation of a central theoretical postulate of evolutionary game theory in oncology: we can treat not only the player, but also the game. Although we concentrate on measuring games played by cancer cells, the measurement methodology we develop can be used to advance the study of games in other microscopic systems by providing a quantitative description of non-cell-autonomous effects.

Tumours are heterogeneous, evolving ecosystems[1,2], comprising subpopulations of neoplastic cells that follow distinct strategies for survival and propagation[3]. The success of a strategy employed by any single neoplastic subpopulation is dependent on the distribution of other strategies, and on various components of the tumour microenvironment, such as cancer-associated fibroblasts (CAFs)[4]. The echinoderm microtubule-associated protein-like 4–anaplastic lymphoma kinase (ALK) fusion—found in approximately 5% of non-small cell lung cancer (NSCLC) patients—leads to constitutive activation of oncogenic tyrosine kinase activity of ALK, thereby 'driving' the disease. Inhibitors of tyrosine kinase activity of ALK (ALK TKIs) have proven to be highly clinically efficacious, inducing tumour regression and prolonging patient survival[5,6]. Unfortunately, virtually all of the tumours that respond to ALK TKIs eventually relapse[7]—an outcome typical of inhibitors of other oncogenic tyrosine kinases[8]. Resistance to ALK TKI, as with most targeted therapies, remains a major unresolved clinical challenge. Despite significant advances in deciphering the resultant molecular mechanisms of resistance[9], the evolutionary dynamics of ALK TKI resistance remains poorly understood. The inability of TKI therapies to completely eliminate tumour cells has been shown to be at least partially attributable to protection by aspects of the tumour microenvironment[10]. CAFs are one of the main non-malignant components of the tumour microenvironment, and the interplay between them and tumour cells is a major contributor to microenvironmental resistance, including cytokine-mediated protection against ALK inhibitors[11].

To study the eco-evolutionary dynamics of these various factors, we interrogated the competition between treatment-naïve cells of the ALK mutant NSCLC cell line H3122 (a 'workhorse' for studies of ALK-positive lung cancer) and a derivative cell line in which we developed resistance to alectinib (a highly effective clinical ALK TKI[12]) by selection in progressively increasing concentrations of the drug[13]. We aimed to come to a quantitative understanding of how these dynamics were affected by clinically relevant concentrations of alectinib (0.5 μM; see ref. [14]) in the presence or absence of CAFs isolated from a lung cancer. To achieve this, we developed an assay for quantifying effective games[15,16] that is of independent interest to the general study of microscopic systems.

Results

Monotypic versus mixed cultures. To establish baseline characteristics, we performed assays in monotypic cultures of parental (alectinib-sensitive) and resistant cell lines with and without alectinib and CAFs. To gather temporally resolved data for inferring growth rates, we used time-lapse microscopy to follow the expansion of therapy-resistant and parental cells, differentially labelled with stable expression of selectively neutral green fluorescent protein (GFP) and mCherry fluorescent proteins, respectively. From the time-series data, we inferred the growth rate with confidence intervals for each of 6 experimental replicates in 4 different experimental conditions (for a total of 24 data points, each with confidence intervals), as seen in Fig. 1. As expected, alectinib inhibited growth rates of parental cells (dimethyl sulfoxide (DMSO) versus alectinib: $P<0.005$; DMSO + CAF versus alectinib + CAF: $P<0.005$), whereas the growth rate of the resistant cells was not affected. In addition, as previously reported[11], CAFs partially rescued growth inhibition of parental cells by alectinib (alectinib versus alectinib + CAF: $P<0.005$; alectinib + CAF versus DMSO: $P<0.005$), without impacting growth rates of resistant cells.

However, we did not limit ourselves to monotypic assays. Our experience observing non-cell-autonomous biological interactions[17] and modelling eco-evolutionary interactions[18–20] in cancer led us to suspect that the heterotypic growth rates would differ from monotypic culture. Cell-autonomous fitness effects are those where the benefits and costs to growth rate are inherent to the cell: the presence of other cells is an irrelevant feature of the microenvironment, and the growth rates from monotypic cultures provide all of

[1]Department of Computer Science, University of Oxford, Oxford, UK. [2]Department of Translational Hematology and Oncology Research, Cleveland Clinic, Cleveland, OH, USA. [3]Department of Radiation Oncology, Moffitt Cancer Center, Tampa, FL, USA. [4]Department of Integrated Mathematical Oncology, Moffitt Cancer Center, Tampa, FL, USA. [5]Department of Cancer Physiology, Moffitt Cancer Center, Tampa, FL, USA. [6]Department of Radiation Oncology, Cleveland Clinic, Cleveland, OH, USA. *e-mail: kaznatcheev.artem@gmail.com; andriy.marusyk@moffitt.org; scottj10@ccf.org

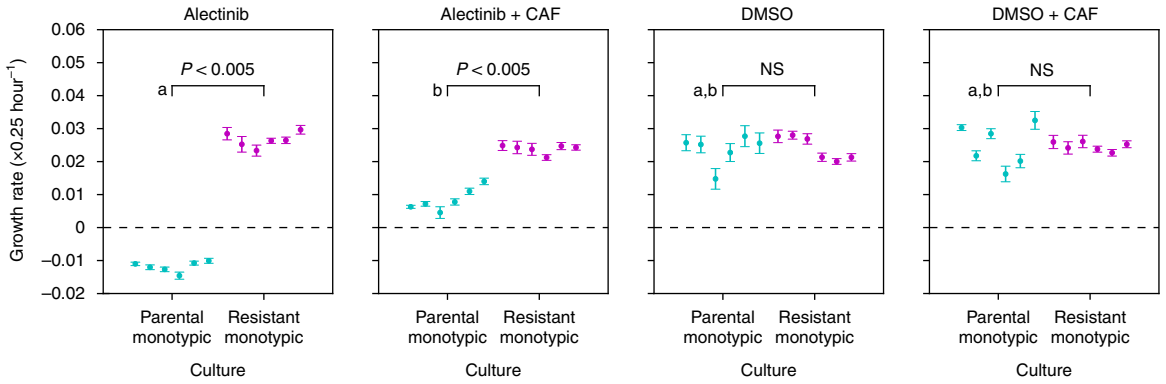

Fig. 1 | Monotypic culture exponential growth rates for parental and resistant cells under the indicated experimental conditions. Confidence intervals on each experimental replicate represent the confidence on the estimate of the growth rate for that single replicate according to the Theil–Sen estimator. Comparisons between experimental conditions (of six replicates each) were made by Wilcoxon rank-sum test. In addition to conditions linked by lines with reported *P* values, conditions labelled by 'a' and 'b' are pairwise distinguishable, with $P < 0.005$. NS, not significant.

the necessary information. Non-cell-autonomous effects[17] allow fitness to depend on a cell's microenvironmental context, including the frequency of other cell types: growth rates need to be measured in competitive fitness assays over a range of seeding frequencies. Other microscopic experimental systems in which frequency-dependent fitness effects have been considered include, but are not limited to: *Escherichia coli*[21,22], yeast[23,24], bacterial symbionts of hydra[25], breast cancer[17] and pancreatic cancer[26]. Hence, we continued our experiments over a range of initial proportions of resistant and parental cells in mixed cultures for each of the four experimental conditions.

Figure 2 shows the resulting growth rates of each cell type in the co-culture experiments for all experimental (colour and shape) and initial conditions (opacity is the parental cell proportion). In the heterotypic culture—unlike monotypic—CAFs slightly improved the growth rates of the parental cells, even in DMSO. More strikingly, even in the absence of drug, resistant cells tend to have a higher growth rate than parental cells in the same environment (that is proportion of parental cells in the co-culture). This is evident from most DMSO points being above the dotted diagonal line ($y=x$) corresponding to equal growth rate of the two types (this is quantified in Fig. 4b and is further discussed in the section 'Leader and Deadlock games in NSCLC').

Frequency dependence in fitness functions. Although not common in cancer biology, competitive fitness assays are a gold standard for studying bacteria. They are typically conducted with a single initial ratio of the two competing cell types. However, in Fig. 2, if we view the initial proportion of parental to resistant cells as a variable parameter represented by opacity, we can see a hint of frequency dependence in both parental and resistant growth rates. This is shown more clearly as a plot of fitness versus the proportion of parental cells in Fig. 3. In all four conditions, we see that the growth rate of the resistant and parental cell lines depends on the initial proportion of parental cells. To capture the principle first-order part of this dependence, we consider a line of best fit between the initial proportion of parental cells and the growth rates. See equations (1)–(8) in Supplementary Section C (or the matrix entries in Fig. 4b) for these lines of best fit. Interpretable versions of these lines of best fit (see Supplementary Section D) can be expressed as a regularized fitness function w_S^C, where $S \in \{P, R\}$ indexes the parental or resistant strategy, and $C \in \{\text{DMSO, DMSO + CAF, alectinib, alectinib + CAF}\}$ indexes the experimental condition. For a description of regularization, see Supplementary Section D. Finally, for a discussion of higher-order fitness functions, see Supplementary Section F.

In three of the conditions, resistant cell growth rates increase with an increased seeding proportion of parental cells, while parental growth rates remain relatively constant (in the case of no CAFs) or slightly increase (for alectinib + CAFs). In DMSO, this suggests that parental cells' fitness is independent of resistant cells: $w_P^{\text{DMSO}} = 0.025$. Parental fitness in DMSO could be well characterized as cell autonomous. However, resistant cells in monotypic culture have approximately the same fitness as parental cells (Fig. 2a), but they benefit from the parental cells in co-culture: $w_R^{\text{DMSO}} = 0.025 + 0.015p$ (where p is the proportion of parental cells). Their fitness has a non-cell-autonomous component. The positive coefficient in front of p suggests commensalism between resistant and parental cells (that is, resistant cells benefit from the interaction with the parental cells, without exerting positive or negative impact on them).

The DMSO + CAF case differs from the other three in that we see a constant—although elevated ($w_R^{\text{DMSO+CAF}} = 0.03$)—growth rate in resistant cells, but a linearly decreasing (in p) growth rate of parental cells: $w_P^{\text{DMSO+CAF}} = 0.025 + 0.01(1-p)$ or, equivalently, $w_P^{\text{DMSO+CAF}} = 0.03 - 0.01\left(\frac{1}{2} - p\right)$. This could be interpreted as CAFs switching the direction of commensalism between parental and resistant cells.

Leader and Deadlock games in NSCLC. The tools of evolutionary game theory (EGT) are well suited for making sense of frequency-dependent fitness[18–20,26–30]. In EGT, a game is the rule mapping the population's strategy distribution to the fitness of individual strategies. Previous work has considered games such as snowdrift[24], stag hunt[25], rock–paper–scissors[21] and public goods[23,26] alongside experiments. Instead, we experimentally operationalize the effective game (see refs. [15,16]) as an assayable hidden variable of a population and its environment. We define the effective game as the game played by an idealized population that shows the same frequency dynamics as the experimental population under consideration. As such, we are not aiming to test EGT as an explanation. Instead, we are defining a game assay to quantitatively describe our system in the language of EGT. In future work, it would be interesting to ask about the best language for describing cancer evolution by testing the game assay against several clearly and well-operationalized alternatives to EGT.

To measure the effective game that describes the non-cell-autonomous interactions in NSCLC, we focus on the gain function (see refs. [20,31] for a theoretical perspective): the difference in growth rate between resistant and parental cells as a function of the proportion of parental cells. The relatively good fit of a linear dependence of growth rates on the parental seeding proportion allows us to describe the interaction as a matrix game—a well-studied

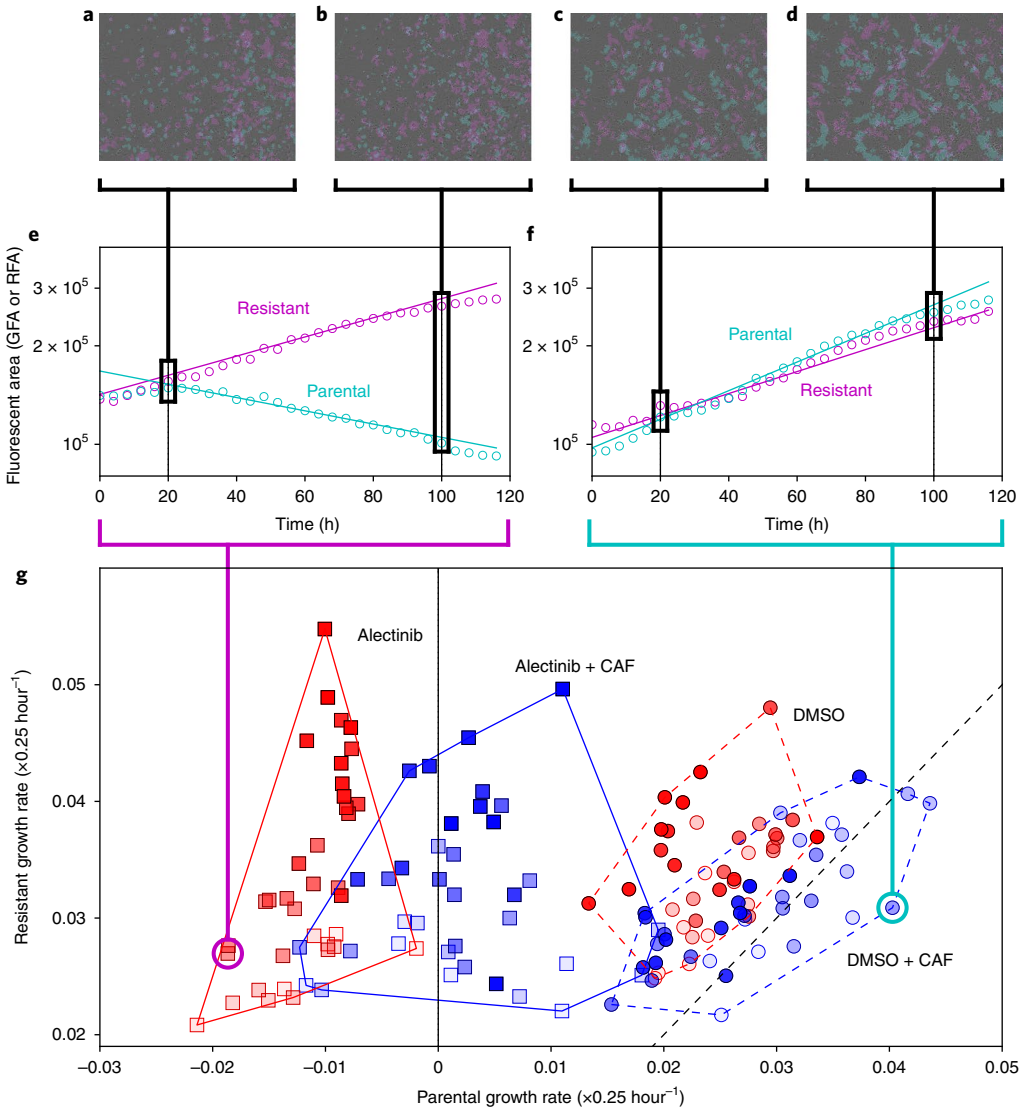

Fig. 2 | Co-culture growth rates across four experimental conditions. a–g, Analysis procedures (**a**–**f**) contributing to the production of **g**. For more detailed discussion, see Supplementary Section B.4. **a**–**d**, In each experimental replicate at each time step, we quantify the population size by the fluorescent area (GFP Fluorescent Area (GFA) or mCherry Fluorescent Area (RFA); see Supplementary Information B.1 and C.1) of each cell type (shown are two different time points per well, from two different wells). **e**,**f**, Together, 30 time-lapse microscopy images (one every 4 h) from each replicate create time-series of parental and resistant population sizes (shown are two example wells). Exponential growth rates (and confidence intervals; omitted) were estimated for each well using the Theil–Sen estimator. These exponential models are shown as solid lines and their slopes serve as the coordinates in **g**. See Fig. 3 for growth-rate confidence intervals and Supplementary Section B.2 for detailed discussion of growth-rate measurements. **g**, Each point is a separate replicate of a competitive fitness assay with the initial proportion of parental cells represented by opacity and the experimental condition represented by shape (DMSO, circle; alectinib, square) and colour (no CAF, red; with CAF, blue). The dotted black line corresponds to the line of equal fitness at $x = y$.

class of evolutionary games (see a description in Fig. 4a). Note that this linearity is not guaranteed to be a good description for arbitrary experimental systems. For example, the game between the two Betaproteobacteria *Curvibacter* species AEP1.3 and *Duganella* species C1.2 was described by a quadratic gain function[25]. If one views our work from the perspective of model selection, in the main text we proceed from the assumption of linearity. Supplementary Section F relaxes this assumption, extends our game assay to nonlinear games and compares linear and nonlinear models with information criteria. Our qualitative results are unchanged, although the exact quantitative results for nonlinear models differ slightly.

Two strategy matrix games have a convenient representation in a two-dimensional game space (see the model in Fig. 4a and Supplementary Section C for details). This is the output of our game assay. We plot the inferred games in a game space spanned by the theoretical fitness advantage a single resistant invader would have if introduced into a parental monotypic culture versus the fitness advantage of a parental invader in a resistant monotypic culture (as shown in Fig. 4b). In this representation, there are four qualitatively different types of games corresponding to the four quadrants, each of which we illustrate with a dynamic flow. We can see that the game corresponding to DMSO + CAF—although quantitatively similar to DMSO—is of a qualitatively different type compared with all three of the other combinations.

We can also convert our inferred fitness functions from Fig. 3 into a payoff matrix. We do this by having each row correspond to a strategy's fitness function with the column entries as the $p = 1$ and $p = 0$ intercepts of this line of best fit. These payoff matrix entries are

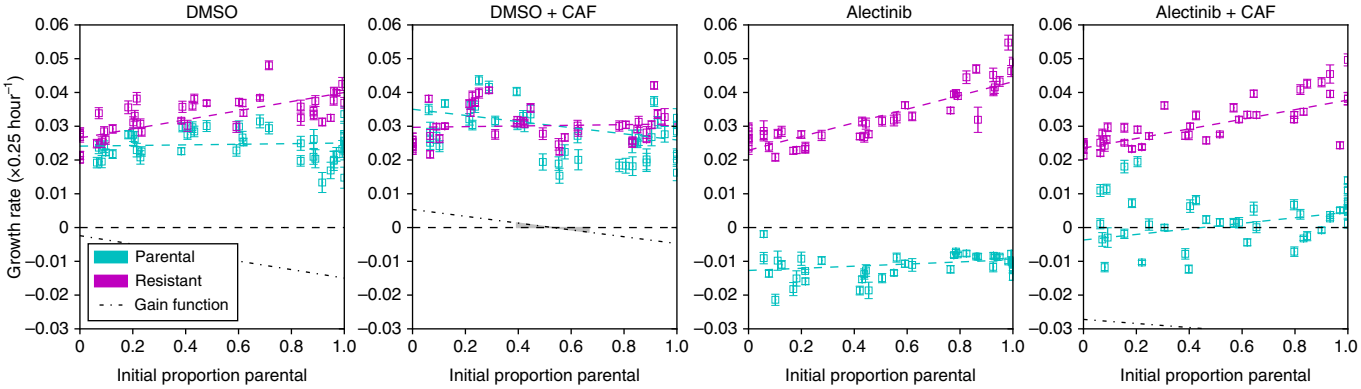

Fig. 3 | Fitness functions for competition of parental versus resistant NSCLC. Each plot shows the growth rate with confidence intervals versus the initial proportion of parental cells. These data were measured in the same way as in Fig. 2. Growth rates of parental and resistant cells are shown as cyan and magenta data points, respectively. Dashed lines represent the linear fitness function of the least-squares best fit; the fit error is visualized in Fig. 4b. The black dot-dashed line is the gain function for parental cells (see Fig. 4a). It is well below the $y=0$ line in the alectinib conditions (indicating the strong advantage of resistance) and thus cut out of the figure. See Supplementary Section C for more discussion and equations for lines of best fit, and Supplementary Section F for alternative fits with nonlinear fitness functions.

abstract phenomenological quantities that could be implemented by various biological or physical processes[15]. If we look at our empirical measurements for DMSO + CAF (upper-right quadrant of Fig. 4b), we see the Leader game, whereas we see Deadlock in the other three cases (we will use DMSO to illustrate the Deadlock game).

The Deadlock game observed in DMSO is in some ways the opposite of the popular Prisoner's Dilemma game (in fact, this is called the anti-Prisoner's Dilemma in ref. [32]). If we interpret parental as cooperate and resistant as defect, similar to the Prisoner's Dilemma, each player wants to defect regardless of what the other player does (because $4.0 > 2.5$ and $2.7 > 2.4$; payoff numbers used in these examples are from the matrix entries we measured in Fig. 4), but hopes that the other player will cooperate (because $4.0 > 2.7$). However, unlike in the Prisoner's Dilemma, mutual cooperation does not Pareto dominate mutual defection (because $2.5 < 2.7$), but is instead strictly dominated by it. Thus, the players are locked into defection. In our system, this corresponds to resistant cells having an advantage over parental cells in DMSO.

The Leader game observed in DMSO + CAF is one of four archetypal 2×2 games in ref. [33], and a social dilemma related to the popular game known as Hawk-dove, Chicken or Snowdrift (in fact, this is called the Benevolent Chicken in ref. [32]). If we interpret parental as 'lead' (for Snowdrift: wait) and resistant as 'work' (for Snowdrift: shovel), similar to Snowdrift, mutual work is better than both leading (because $3.0 > 2.6$) and thus no work being done (for Snowdrift: both waiting and thus not getting out of the snowdrift), but each player would want to lead while the other works (because $3.5 > 3.0$). However, unlike Snowdrift, mutual work is not better than the 'sucker's payoff' of working while the other player leads (because $3.1 > 3.0$). In ref. [33], this is seen as a tension with a player switching from a 'natural' point of mutual work to lead and thus benefit both players ($3.5 > 3.0$; $3.1 > 3.0$), but if the second player also does the same and becomes a leader, all benefit disappears (because 2.6 is the smallest payoff). In our system, this corresponds to cells in the tumour experiencing selective pressure to lose some but not all of their resistance in DMSO + CAF.

Note that the above intuitive stories are meant as heuristics, and the effective games that we measure are summaries of population-level properties[15,16]: the population is the player and the two types of cancer cells are the strategies. This means that the matrix entries should not be interpreted as direct interactions between cells, but as general couplings between subpopulations corresponding to different strategies. The coupling term includes not only direct interactions, but also indirect effects due to spatial structure, diffusible goods, contact inhibition and so on. However, this does not mean that an effective game is not interpretable. For example, the Deadlock game captures the phenomenon of the resistant population always being fitter than the parental population (for example, in DMSO). We noted this effect intuitively in Fig. 2 (also see the section 'Cost of resistance') from replicates being above the $y=x$ diagonal. Measuring a Deadlock game for DMSO with confidence intervals that do not extend outside the bottom-right quadrant of the game space in Fig. 4b allows us to show the statistical significance of our previous intuitive understanding. In other words, effective games allow us to quantify frequency-dependent differences in growth rates.

Discussion

Cost of resistance. The classic model of resistance posits that the resistant phenotype receives a benefit in drug (in our case: alectinib or alectinib + CAF) but is neutral, or even carries an inherent cost, in the absence of treatment (DMSO or DMSO + CAF). For example, experimentalists frequently regard resistance-granting mutations as selectively neutral in the absence of drugs, and the modelling community often goes further by considering explicit costs such as upregulating drug efflux pumps, investing in other defensive strategies or lowering the growth rate by switching to suboptimal growth pathways[3,34]. If we limited ourselves to the monotypic assays of Fig. 1, our observations would be consistent with this classic model of resistance. However, in co-culture, we observed that resistant cells have higher fitness than parental cells in the same environment, even in the absence of a drug. This is not consistent with the classic model of resistance. This higher fitness of resistant cells might not surprise clinicians as much as biologists: in clinical experience, tumours that have acquired resistance are often more aggressive than before they were treated, even in the absence of drugs. See Supplementary Section A.3 for a contrast of the biologist's and clinician's view of resistance in this context.

Treating the game. Measuring a linear gain function has enabled us to develop an assay that represents the interdependence between parental and resistant cells as a matrix game. Experimentally cataloguing these games allows us to support existing theoretical work in mathematical oncology that considers treatment (or other environmental differences) as changes between qualitatively different game regimes[18–20,30]. In this framework, treatment has the goal

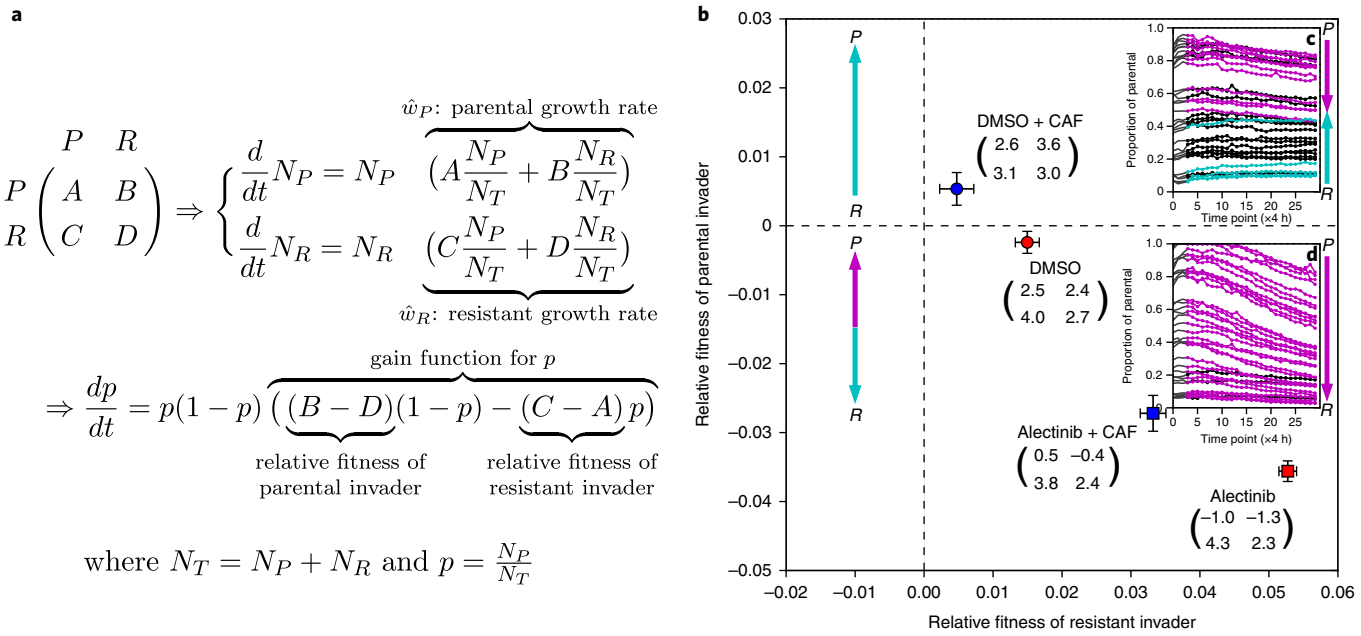

Fig. 4 | Measured games. a, Replicator dynamics. Consider an idealized population of two strategies in a competitive co-culture: parental (*P*) and resistant (*R*). When a subpopulation of *P* interacts with *P*, the subpopulation experiences a fitness effect *A*. When *P* interacts with *R*, *P* experiences fitness effect *B* and *R* experiences fitness effect *C*. Two *R*s interact with fitness effect *D*. These effects are summarized in the matrix. This can be interpreted as an idealized exponential growth model for the number of parental (N_P) and resistant (N_R) cells. The dynamics of the proportion of parental cells $p = \frac{N_P}{N_P + N_R}$ over time is described by the replicator equation (bottom). In Supplementary Section E, we discuss a purely experimental interpretation based on ref. [15]. **b**, Mapping of the four measured in vitro games into game space. The *x* axis is the relative fitness of a resistant focal in a parental monotypic culture: $C - A$; the *y* axis is the relative fitness of a parental focal in a resistant monotypic culture: $B - D$. Games measured in our experimental system are given as specific points, with error bars based on the goodness of fit of linear fitness functions in Fig. 3. The games corresponding to our conditions are given as matrices (with entries multiplied by a factor of 100) by their label. See Supplementary Section C for more details. The game space is composed of four possible dynamical regimes—one for each quadrant. The typical dynamics of each dynamic regime is represented as a qualitative flow diagram between *P* and *R*: an upward cyan arrow corresponds to an increase in the parental proportion and a downward magenta arrow corresponds to an increase in the resistant proportion. **c**,**d**, In the case of the two dynamic regimes observed in our NSCLC system, we also include insets of measured dynamics—experimental time-series of the proportion of parental cells for DMSO + CAF (**c**) and alectinib + CAF (**d**). Each line corresponds to the time dynamics of a separate well. A line is coloured magenta if the proportion of resistant cells increased from the start to the end, cyan if the proportion of parental cells increased and black if the proportions were statistically indistinguishable at the start and end (where start and end are defined as the first and last 5 time points (20 h)). See Supplementary Fig. 1 for proportion dynamics of all four games and Supplementary Fig. 2 for density dynamics and their correspondence to the exponential growth model from Fig. 4a.

not to directly target cells in the tumour, but instead to perturb the parameters of the game they are playing to allow evolution to steer the tumour towards a more desirable result (for example, see refs. [18–20,30,35,36]). Empirically, this principle has inspired or built support for interventions, such as buffer therapy[37], vascular renormalization therapy[38] and adaptive therapy[39], that target the microenvironment and interactions instead of just attacking the cancer cell population. The success of the trial in ref. [39] suggests that therapeutic strategies based on modulating competition dynamics are feasible. This highlights the need for a formal experimental method such as our game assay that directly measures the games that cancer plays and tracks whether and how they change due to treatment.

In our system, we can view an untreated tumour as similar to DMSO + CAF, and thus following the Leader game. Treating with alectinib (a move to alectinib + CAF) or eliminating CAFs through a stromal-directed therapy (a move to DMSO) moves the game into the lower-right quadrant of Fig. 4b, and it becomes a Deadlock game. Not only are these games quantitatively different among the four environmental conditions (see Fig. 4b) but they are also of two qualitatively different types. To our knowledge, neither of the Leader and Deadlock games is considered in the previous EGT literature in oncology. Given that the Deadlock of drug-resistant over drug-sensitive cells is a challenge for classic models of resistance, we would be particularly interested in theoretical models of resistance that produce the Deadlock game. In addition to challenging theorists by adding two new entries to the catalogue of games that cancers play, this switch allows us to show that the theoretical construct of EGT (that treatment can qualitatively change the type of game) has a direct experimental implementation. Unfortunately, neither of our in vitro games would lead to a therapeutically desirable outcome if they occurred in a patient.

Heterogeneity and latent resistance. A particularly important difference between Leader and Deadlock dynamics is the existence of an internal fixed point in Leader but not in Deadlock. Fixed points are a property of equilibrium dynamics: in the most general case, even on very long timescales, these fixed points might not be realized due to the evolutionary constraints of population size[40] or computation[41,42]. Thus, it is important to check to what extent this qualitative difference can translate to a quantitative difference in finite time horizons. In our system, we can see a quantitative difference in the convergence towards the fixed point in the DMSO + CAF condition of Fig. 4c, and no such convergence in the other three cases (Fig. 4d for alectinib + CAF; Supplementary Fig. 1). Since the strength of selection (the magnitude of the gain function) is small near a fixed point, the change in *p* also slows in the DMSO + CAF condition. We

provide a more robust analysis of this in Supplementary Sections C and F. It would be of interest for future work to study the long-term experimental stability of these fixed points.

Since the DMSO + CAF condition is our closest to an untreated patient, it might have important consequences for latent resistance. Many classical models of resistance assume a rare pre-existent mutant taking over the population after the introduction of a drug. However, in our experimental system, if the resistant strategy is pre-existent, negative frequency-dependent selection will push the population towards a stable polyclonal tumour of resistant and sensitive cells before the introduction of a drug. This allows for much higher levels of pre-existing heterogeneity in resistance than predicted by the classical picture. As such, we urge theorists to reconsider the assumption of the rare pre-existing resistant clone.

Of course, our results are for a single in vitro system. However, if similar games occur in vivo and/or for other cancers, such pre-existing heterogeneity could be a possible evolutionary mechanism behind the speed and robustness of treatment resistance to targeted therapies in patients. This could help explain the ubiquity and speed of resistance that undermines our abilities to cure patients or control their disease in the long term. We will not know this unless we set out to quantify the non-cell-autonomous processes in cancer. Building a catalogue of the games cancers play—by adopting our game assay in other cancers, and other experimental contexts—can help resolve this and other questions.

Methods

Cell lines. The H3122 cell line was obtained from E. Haura (Moffitt Cancer Center). Cell line identity was validated by the Moffitt Cancer Center Molecular Genetics core facility using short tandem repeats analysis. Primary lung CAFs were obtained from the laboratory of S. Antonia (Moffitt Cancer Center), following the protocols approved by the University of South Florida Institutional Review Board. CAFs were isolated as described previously[43] and expanded for 3–10 passages before the experiments. The alectinib-resistant derivative cell line was obtained through escalating inhibitor concentration protocol, as described previously[13]. Alectinib-sensitive parental H3122 cells were cultured in DMSO for the same length of time as the alectinib-resistant derivate.

Stable GFP- and mCherry-expressing derivative cell H3122 cell lines were obtained, respectively, through lentiviral transduction with pLVX-AcGFP (Clontech) and mCherry vectors (obtained from K. Mitsiades at the Dana–Farber Cancer Institute). We cultured both H3122 cells and CAFs in Roswell Park Memorial Institute (RPMI) media (Gibco; Thermo Fisher Scientific), supplemented with 10% foetal bovine serum (Serum Source). Regular tests for *Mycoplasma* contamination were performed with a MycoScope PCR based kit (Genlantis).

Experimental set-up. The cells were harvested on reaching 70% confluence and counted using a Countess II automatic cell counter (Invitrogen). CAFs were counted manually to avoid segmentation artefacts. Mixtures of parental and resistant H3122 cells were prepared at 8 different ratios: all resistant, resistant-to-parental ratios of 9:1, 4:1, 3:2, 2:3, 1:4 and 1:9, and all parental. For the determination of competitive growth rates, 2,000 H3122 cells from the 8 mixtures were seeded with or without 500 CAF cells in 50 µl RPMI media per well into 384-well plates (Corning; catalogue number 7200655), with different ratios of differentially labelled parental and alectinib-resistant variants (6 wells were used for each resistant-to-parental ratio in each of the 4 conditions). Then, 20 h after seeding, alectinib (ChemieTek) or DMSO vehicle control, diluted in 20 µl RPMI, was added to each well, to achieve a final alectinib concentration of 500 nM l^{-1} (ref. [14]). Time-lapse microscopy measurements were performed every 4 h in phase-contrast white light, as well as green and red fluorescent channels using an IncuCyte ZOOM system (Essen BioScience).

Game assay. We used the exponential growth rate in the fluorescent area of the two fluorescent channels as our measure of fitness. To minimize the impact of growth inhibition by confluency, we analysed the competitive dynamics during the first 5 d of culture, when the cell population was expanding exponentially. We learned the growth rate, along with a confidence interval, from the time series of the population size in each well using the Theil–Sen estimator. More details on, and justification of, this measure of fitness are available in Supplementary Section B.2.

Since raw population sizes have different units (GFP fluorescent area (GFA) versus mCherry fluorescent area (RFA)), we converted them to common cell-number units (CNU) by learning the linear transform that scales GFA and RFA into CNU. We defined proportions based on this common CNU as $p = N_P/(N_P + N_R)$, where $N_{\{P,R\}}$ is the CNU size of parental and resistant populations. The transform of GFA to RFA into CNU is associated with an error that is propagated to measures of p as σ_p.

To measure the fitness functions, we plotted the fitness of each cell type in each well versus the seeding proportion (p) of parental cells in Fig. 3. The x axis proportion of parental cells (p) was computed from the first time point. We estimated the line of best fit and error on parameters for this data using least squares weighted by the inverse of the error on each data point. For the exact lines of best fit, see Supplementary Section C.3.

The $p = 0$ and $p = 1$ intercepts of the lines of best fit serve as the entries of the game matrices. Note that in Fig. 4b, we multiplied the entries by 100 for easier presentation. The game points were calculated from the matrices as $x = C - A$ and $y = B - D$, and the error was propagated from the error estimates on the parameters of lines of best fit.

Reporting Summary. Further information on research design is available in the Nature Research Reporting Summary linked to this article.

Code availability

Image analysis code is available on GitHub at https://github.com/kaznatcheev/CV4Microscopy. The game assay analysis code is available on GitHub at https://github.com/kaznatcheev/GameAssay.

Data availability

Due to size constraints, raw image data from experiments are available upon request. Post-image processing data (that is, population size time-series for each experimental replicate) are available on GitHub at https://github.com/kaznatcheev/GameAssay.

Received: 23 August 2017; Accepted: 22 November 2018;
Published online: 18 February 2019

References

1. Merlo, L. M. F., Pepper, J. W., Reid, B. J. & Maley, C. C. Cancer as an evolutionary and ecological process. *Nat. Rev. Cancer* **6**, 924–935 (2006).
2. Heppner, G. H. Tumor heterogeneity. *Cancer Res.* **44**, 2259–2265 (1984).
3. Ibrahim-Hashim, A. et al. Defining cancer subpopulations by adaptive strategies rather than molecular properties provides novel insights into intratumoral evolution. *Cancer Res.* **77**, 2242–2254 (2017).
4. Scott, J. & Marusyk, A. Somatic clonal evolution: a selection-centric perspective. *Biochim. Biophys. Acta* **1867**, 139–150 (2017).
5. Shaw, A. T. et al. Crizotinib versus chemotherapy in advanced ALK-positive lung cancer. *N. Engl. J. Med.* **368**, 2385–2394 (2013).
6. Peters, S. et al. Alectinib versus crizotinib in untreated ALK-positive non-small-cell lung cancer. *N. Engl. J. Med.* **377**, 829–838 (2017).
7. Shaw, A. T. & Engelman, J. A. ALK in lung cancer: past, present, and future. *J. Clin. Oncol.* **31**, 1105–1111 (2013).
8. Gillies, R. J., Verduzco, D. & Gatenby, R. A. Evolutionary dynamics of carcinogenesis and why targeted therapy does not work. *Nat. Rev. Cancer* **12**, 487–493 (2012).
9. Katayama, R., Lovly, C. M. & Shaw, A. T. Therapeutic targeting of anaplastic lymphoma kinase in lung cancer: a paradigm for precision cancer medicine. *Clin. Cancer Res.* **21**, 2227–2235 (2015).
10. Marusyk, A. et al. Spatial proximity to fibroblasts impacts molecular features and therapeutic sensitivity of breast cancer cells influencing clinical outcomes. *Cancer Res.* **76**, 6495–6506 (2016).
11. Yamada, T. et al. Paracrine receptor activation by microenvironment triggers bypass survival signals and ALK inhibitor resistance in EML4–ALK lung cancer cells. *Clin. Cancer Res.* **18**, 3592–3602 (2012).
12. Ou, S.-H. I. et al. Alectinib in crizotinib-refractory ALK-rearranged non-small-cell lung cancer: a phase II global study. *J. Clin. Oncol.* **34**, 661–668 (2015).
13. Dhawan, A. et al. Collateral sensitivity networks reveal evolutionary instability and novel treatment strategies in ALK mutated non-small cell lung cancer. *Sci. Rep.* **7**, 1232 (2017).
14. Seto, T. et al. CH5424802 (RO5424802) for patients with ALK-rearranged advanced non-small-cell lung cancer (AF-001JP study): a single-arm, open-label, phase 1–2 study. *Lancet Oncol.* **14**, 590–598 (2013).
15. Kaznatcheev, A. Two conceptions of evolutionary games: reductive vs effective. Preprint at https://www.biorxiv.org/content/early/2017/12/11/231993 (2017).
16. Kaznatcheev, A. Effective games and the confusion over spatial structure. *Proc. Natl Acad. Sci. USA* **115**, E1709 (2018).
17. Marusyk, A. et al. Non-cell autonomous tumor-growth driving supports sub-clonal heterogeneity. *Nature* **514**, 54–58 (2014).
18. Basanta, D. et al. Investigating prostate cancer tumour–stroma interactions: clinical and biological insights from an evolutionary game. *Br. J. Cancer* **106**, 174–181 (2012).
19. Kaznatcheev, A., Scott, J. G. & Basanta, D. Edge effects in game-theoretic dynamics of spatially structured tumours. *J. R. Soc. Interface* **12**, 20150154 (2015).

20. Kaznatcheev, A., Vander Velde, R., Scott, J. G. & Basanta, D. Cancer treatment scheduling and dynamic heterogeneity in social dilemmas of tumour acidity and vasculature. *Br. J. Cancer* **116**, 785–792 (2017).
21. Kerr, B., Riley, M. A., Feldman, M. W. & Bohannan, B. J. M. Local dispersal promotes biodiversity in a real-life game of rock–paper–scissors. *Nature* **418**, 171–174 (2002).
22. Maddamsetti, R., Lenski, R. E. & Barrick, J. E. Adaptation, clonal interference, and frequency-dependent interactions in a long-term evolution experiment with *Escherichia coli*. *Genetics* **200**, 619–631 (2015).
23. MacLean, R. C. & Gudelj, I. Resource competition and social conflict in experimental populations of yeast. *Nature* **441**, 498–501 (2006).
24. Gore, J., Youk, H. & Van Oudenaarden, A. Snowdrift game dynamics and facultative cheating in yeast. *Nature* **459**, 253–256 (2009).
25. Li, X.-Y. et al. Which games are growing bacterial populations playing? *J. R. Soc. Interface* **12**, 20150121 (2015).
26. Archetti, M., Ferraro, D. A. & Christofori, G. Heterogeneity for IGF-II production maintained by public goods dynamics in neuroendocrine pancreatic cancer. *Proc. Natl Acad. Sci. USA* **112**, 1833–1838 (2015).
27. Maynard Smith, J. & Price, G. R. The logic of animal conflict. *Nature* **246**, 15–18 (1973).
28. Tomlinson, I. P. & Bodmer, W. F. Modelling the consequences of interactions between tumour cells. *Br. J. Cancer* **75**, 157–160 (1997).
29. Tomlinson, I. P. Game-theory models of interactions between tumour cells. *Eur. J. Cancer* **33**, 1495–1500 (1997).
30. Archetti, M. Evolutionary game theory of growth factor production: implications for tumour heterogeneity and resistance to therapies. *Br. J. Cancer* **109**, 1056–1062 (2013).
31. Peña, J., Lehmann, L. & Nöldeke, G. Gains from switching and evolutionary stability in multi-player matrix games. *J. Theor. Biol.* **346**, 23–33 (2014).
32. Robinson, D. & Goforth, D. *The Topology of the 2×2 Games: a New Periodic Table* Vol. 3 (Psychology Press, New York, 2005).
33. Rapoport, A. Exploiter, leader, hero, and martyr: the four archetypes of the 2×2 game. *Syst. Res. Behav. Sci.* **12**, 81–84 (1967).
34. Anderson, A. R. A., Weaver, A. M., Cummings, P. T. & Quaranta, V. Tumor morphology and phenotypic evolution driven by selective pressure from the microenvironment. *Cell* **127**, 905–915 (2006).
35. Nichol, D. et al. Steering evolution with sequential therapy to prevent the emergence of bacterial antibiotic resistance. *PLoS Comput. Biol.* **11**, e1004493 (2015).
36. Basanta, D., Scott, J. G., Rockne, R., Swanson, K. R. & Anderson, A. R. A. The role of IDH1 mutated tumour cells in secondary glioblastomas: an evolutionary game theoretical view. *Phys. Biol.* **8**, 015016 (2011).
37. Gatenby, R. A., Gawlinski, E. T., Gmitro, A. F., Kaylor, B. & Gillies, R. J. Acid-mediated tumor invasion: a multidisciplinary study. *Cancer Res.* **66**, 5216–5223 (2006).
38. Jain, R. K. Normalizing tumor microenvironment to treat cancer: bench to bedside to biomarkers. *J. Clin. Oncol.* **31**, 2205–2218 (2013).
39. Zhang, J., Cunningham, J. J., Brown, J. S. & Gatenby, R. A. Integrating evolutionary dynamics into treatment of metastatic castrate-resistant prostate cancer. *Nat. Commun.* **8**, 1816 (2017).
40. Gerlee, P. & Altrock, P. M. Extinction rates in tumour public goods games. *J. R. Soc. Interface* **14**, 20170342 (2017).
41. Conitzer, V. The exact computational complexity of evolutionarily stable strategies. In *International Conference on Web and Internet Economics* 96–108 (Springer, 2013).
42. Kaznatcheev, A. Computational complexity as an ultimate constraint on evolution. Preprint at https://www.biorxiv.org/content/early/2018/06/18/187682 (2018).
43. Mediavilla-Varela, M., Boateng, K., Noyes, D. & Antonia, S. J. The anti-fibrotic agent pirfenidone synergizes with cisplatin in killing tumor cells and cancer-associated fibroblasts. *BMC Cancer* **16**, 176 (2016).

Acknowledgements

J.G.S. acknowledges the NIH Loan Repayment Programs for generous support of his research in general, as well as Miles for Moffitt and the NIH Case Comprehensive Cancer Center (support grant P30CA043703), and the Calabresi Clinical Oncology Research Program, National Cancer Institute (award number K12CA076917). We also thank M. Abazeed, P. Jeavons and K. Kaznatcheev for helpful feedback and discussions.

Author contributions

A.K., J.P., A.M. and J.G.S. conceived and designed the study. J.P. and A.M. performed the experiments. A.K. designed the mathematical model, wrote the image analysis and game assay code, and analysed the data. A.K., A.M. and J.G.S. wrote the main text. A.K. and J.P. wrote the Supplementary Information. D.B., A.M. and J.G.S. supervised the project. All authors discussed the results and implications, commented on the work at all stages and approved the final submission.

Competing interests

The authors declare no competing interests.

Additional information

Supplementary information is available for this paper at https://doi.org/10.1038/s41559-018-0768-z.

Reprints and permissions information is available at www.nature.com/reprints.

Correspondence and requests for materials should be addressed to A.K., A.M. or J.G.S.

Publisher's note: Springer Nature remains neutral with regard to jurisdictional claims in published maps and institutional affiliations.

nature research

Corresponding author(s): Jacob G. Scott

Reporting Summary

Nature Research wishes to improve the reproducibility of the work that we publish. This form provides structure for consistency and transparency in reporting. For further information on Nature Research policies, see Authors & Referees and the Editorial Policy Checklist.

Statistical parameters

When statistical analyses are reported, confirm that the following items are present in the relevant location (e.g. figure legend, table legend, main text, or Methods section).

n/a	Confirmed	
☐	☒	The exact sample size (*n*) for each experimental group/condition, given as a discrete number and unit of measurement
☐	☒	An indication of whether measurements were taken from distinct samples or whether the same sample was measured repeatedly
☐	☒	The statistical test(s) used AND whether they are one- or two-sided *Only common tests should be described solely by name; describe more complex techniques in the Methods section.*
☐	☒	A description of all covariates tested
☐	☒	A description of any assumptions or corrections, such as tests of normality and adjustment for multiple comparisons
☐	☒	A full description of the statistics including central tendency (e.g. means) or other basic estimates (e.g. regression coefficient) AND variation (e.g. standard deviation) or associated estimates of uncertainty (e.g. confidence intervals)
☐	☒	For null hypothesis testing, the test statistic (e.g. *F*, *t*, *r*) with confidence intervals, effect sizes, degrees of freedom and *P* value noted *Give P values as exact values whenever suitable.*
☒	☐	For Bayesian analysis, information on the choice of priors and Markov chain Monte Carlo settings
☒	☐	For hierarchical and complex designs, identification of the appropriate level for tests and full reporting of outcomes
☒	☐	Estimates of effect sizes (e.g. Cohen's *d*, Pearson's *r*), indicating how they were calculated
☐	☒	Clearly defined error bars *State explicitly what error bars represent (e.g. SD, SE, CI)*

Our web collection on statistics for biologists may be useful.

Software and code

Policy information about availability of computer code

Data collection	Raw data are available on request. Processed image data is available via github: https://github.com/kaznatcheev/TLM_FA
Data analysis	Analysis software available via github: https://github.com/kaznatcheev/GameAssay

For manuscripts utilizing custom algorithms or software that are central to the research but not yet described in published literature, software must be made available to editors/reviewers upon request. We strongly encourage code deposition in a community repository (e.g. GitHub). See the Nature Research guidelines for submitting code & software for further information.

Data

Policy information about availability of data

All manuscripts must include a data availability statement. This statement should provide the following information, where applicable:

- Accession codes, unique identifiers, or web links for publicly available datasets
- A list of figures that have associated raw data
- A description of any restrictions on data availability

Due to size constraints, raw image data from experiments are available upon request.
Image analysis code is available on GitHub at https://github.com/kaznatcheev/TLM_FA.
Post-image processing data (i.e. population size time-series for each experimental replicate) is available on GitHub at https://github.com/kaznatcheev/GameAssay.

Field-specific reporting

Please select the best fit for your research. If you are not sure, read the appropriate sections before making your selection.

☒ Life sciences ☐ Behavioural & social sciences ☐ Ecological, evolutionary & environmental sciences

For a reference copy of the document with all sections, see nature.com/authors/policies/ReportingSummary-flat.pdf

Life sciences study design

All studies must disclose on these points even when the disclosure is negative.

Sample size	There was no need for power calculations. We used four images from each well to calculate error, and reported absolute error. For the tests of statistical difference in figure 1 (the only place we report a p-value), triplicate experiments were performed.
Data exclusions	no data were excluded
Replication	Experiments were reproduced in three independent biological replicates, each with multiple technical replicates.
Randomization	n/a
Blinding	n/a

Reporting for specific materials, systems and methods

Materials & experimental systems

n/a	Involved in the study
☒	☐ Unique biological materials
☒	☐ Antibodies
☐	☒ Eukaryotic cell lines
☒	☐ Palaeontology
☒	☐ Animals and other organisms
☒	☐ Human research participants

Methods

n/a	Involved in the study
☒	☐ ChIP-seq
☒	☐ Flow cytometry
☒	☐ MRI-based neuroimaging

Eukaryotic cell lines

Policy information about cell lines

Cell line source(s)	H3122 were obtained from the Haura lab, Fibroblasts were obtained from the Antonia laboratory at Moffitt Cancer Center.
Authentication	We used standard STR based cell identity validation through molecular biology core at Moffitt Cancer Center.
Mycoplasma contamination	The cells were periodically tested for mycoplasma contamination.
Commonly misidentified lines (See ICLAC register)	none